^{13}C NMR Study of the Conformation and Dynamics of Bisphenol A Polycarbonate

P. Mark Henrichs*,†

Corporate Research Laboratories, Eastman Kodak Company, Rochester, New York 14650-2021

V. A. Nicely*

Research Laboratories, Eastman Chemical Company, Kingsport, Tennessee 37662

Received April 19, 1990

ABSTRACT: Local chain dynamics in solid Bisphenol A polycarbonate (BPAPC) was studied through its effect on the line width of the ^{13}C NMR signals of samples spinning at the magic angle. The homogeneous line widths, which are associated in part with motion, were separated from the inhomogeneous line widths, which have causes such as a distribution of local packing environments, through generation of a spin-echo train. The line widths of the protonated aromatic carbons depended strongly on temperature. A motion that could cause such temperature-dependent line widths is ring flipping. Ring flipping would not contribute to the widths of carbons lying on the flipping axis, and indeed the widths of the resonances from the nonprotonated carbons were temperature independent. The temperature of maximum line broadening of the signals from the proton-bearing carbons is consistent with an activation energy of 8–9 kcal/mol. Three-fold rotation of the methyl groups is adequate to explain the width of the signals from the methyl carbon at low temperature. However, isotropic motion of the methyls with a temperature-dependent amplitude, in addition to methyl rotation, is not ruled out.

The temperature and structure dependence of the mechanical, electrical, and transport characteristics of polymers implies that there is a molecular origin of these properties. Some of the attributes probably derive from the dynamic properties of the polymer chain. It is generally believed that, above the glass transition temperature, there is cooperative motion of large segments of the polymer chain and its neighboring chains. There is some evidence that properties such as impact strength and diffusion are associated below the glass transition temperature with motions of localized, relatively small sections of the polymer chain.[1-5]

Of the spectroscopic tools for determination of the molecular origins of polymer dynamic properties, NMR spectroscopy is one of the most developed. However, most studies with NMR give only general information about motion in the sample. Proton NMR spectroscopy, for example, lacks the specificity to identify the mobile domains or moieties in polymer chains unless signals from some portions of the chain have been eliminated by isotopic substitution. The most common method of inferring the relation of local chain motions to macroscopic polymer properties is by observation of the effect of substitutional replacement of key portions of the polymer repeat unit on the properties.

By contrast to proton NMR spectroscopy, deuterium NMR spectroscopy is very powerful in clarifying the nature of local chain motions in polymers and is highly site specific in that signals are obtained only from positions that have been labeled with deuterium. Unfortunately, the specificity is obtained at the cost of special synthetic procedures to prepare labeled samples. Polymers as they come from industrial production cannot be used at all.

^{13}C NMR spectroscopy also provides site-specific information about motion because, with high-power decoupling and magic-angle spinning, resolved signals from chemically different carbons often are observed. Chain motion affecting each carbon site can be explored selectively through properties of the nuclei such as their nuclear relaxation times. Carbon NMR spectroscopy normally does not require isotopically labeled samples.

The widths of the ^{13}C NMR resonances have only rarely been used as a source of information about chain motion in polymers. The primary impediment is that the motional contribution to the line width of a ^{13}C nucleus in an amorphous polymer is generally small. Typically, an observed signal from an amorphous polymer is broadened more by the spread in absorption frequencies resulting from the multitude of local environments for the nuclei than by chain motion. The line width caused by the spread in frequencies is an example of inhomogeneous broadening of the NMR signal. The motional contribution to line broadening is an example of homogeneous broadening.

In the presence of severe inhomogeneous line broadening the homogeneous line broadening must be determined with a suitable spin-echo method. NMR line widths are inversely proportional to the rate at which the NMR signal decays as a function of time. The essential feature of a spin-echo experiment is that the decay related to the inhomogeneous broadening of a signal can be reversed with application of an appropriate NMR pulse.[6] In a set of experiments in which the decay related to inhomogeneous broadening has been cancelled through the formation of a spin echo, the much slower decay caused by motion can be detected. The spin-echo method is illustrated here for a typical synthetic polymer, Bisphenol A polycarbonate (BPAPC). Conclusions about the nature of local motion in Bisphenol A polycarbonate are inferred from the results.

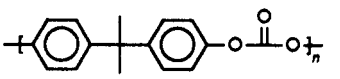

Bisphenol A polycarbonate (BPAPC)

Experimental Section

Samples. Three different materials were examined. One was Lexan 145, used as received. A second consisted of Merlon M40

† Present address: Exxon Chemical Co., Baytown Polymers Center, 5200 Bayway Drive, Baytown, TX 77522-5200.

0024-9297/91/2224-2506$02.50/0

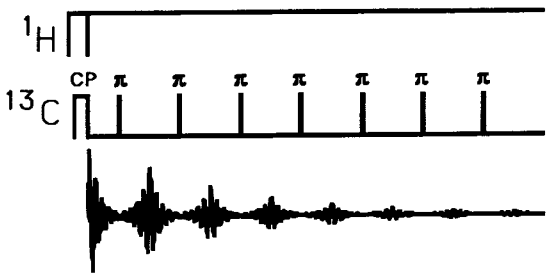

Figure 1. Pulse program used for generation of "spike" ^{13}C NMR spectra. Sample spinning is coordinated with the pulse cycle so that each 180° pulse occurs at the same point in the cycle. Usually there were 32 rotation cycles between each pair of 180° pulses.

pellets, also used as received. The third was a film that was pressed from the Merlon pellets at 200° and quenched in ice.

The polymers were packed with a little KBr and alumina into a sample spinner made of sapphire. The bromine signal of the KBr was used for adjustment of the angle of magic-angle spinning.[7]

NMR Spectra. ^{13}C NMR spectra were generated with a Bruker CXP-100 spectrometer equipped with an Aspect 3000 computer and a magic-angle-spinning probe from Doty Scientific. The 90° pulse times for both carbons and protons were normally 4.5 μs. The sample temperature was controlled with the standard Bruker equipment. The temperature on the controller was calibrated against the temperature of a thermocouple inserted in the exit gas just above the sample spinner in a probe on the bench top. Reported temperatures are believed to be accurate to within 2 °C.

A typical spin-echo experiment began with generation of transverse carbon magnetization by cross-polarization. A series of spin echoes was then created with a train of 180° pulses (Figure 1). The signal was detected continuously throughout the echo train. The phase of the pulse train was alternated between 0° and 180° with respect to the cross-polarization pulse on alternate scans to cancel out pulse artifacts.

The actual spinning rate was chosen to minimize interference of spinning sidebands with the signals of interest. The pulse spacing was then chosen to be an exact multiple of the spinning period. Typically the multiplier was 32. With this multiplier the pulses in the echo train were spaced about 10 ms apart.

Synchronization of the pulse train and sample spinning was essential.[8-12] Improper synchronization would have led to unwanted modulation of the echo train.[8] This modulation would have led to additional peaks in the final spectrum separated from the primary peaks by the modulation frequency. Correspondingly, drift in the spinning speed would have led to artificial suppression of the echo train and unwanted broadening of the peaks in the final spectrum. To minimize the effect of drift in the spinning speed, we used spinning rates of only 1500–2000 Hz and held the pressure of the drive gas constant with one or more pressure controllers. Normally the spinning speed remained within 5 Hz of the nominal value during the course of an experiment.

The homogeneous line width of a particular signal in the spectrum is inversely proportional to the decay rate of the component of the spin echo corresponding to that signal. In principle, the decay rates of each of the signals in the spectrum could have been determined with Fourier transformation of the latter half of each echo and measurement of the rate at which each spectral component decayed. Instead, we used an alternative procedure involving Fourier transformation of the entire train of spin echoes together.[13-15] The train of spin echoes is analogous to the train of rotational echoes generated by magic-angle spinning.[16,17] For the latter the "spun" echoes lead to spinning sidebands in the spectrum after Fourier transformation. Likewise, Fourier transformation of a spin-echo train leads to an "echo" or "spike" spectrum broken into a series of sidebands. The widths of the individual spikes are effectively the homogeneous line widths. The difference between the standard ^{13}C spectrum of solid BPAPC and the echo spectrum is illustrated in Figure 2.

The spikes in the spectrum derived from the spin-echo train differ from the sidebands generated by magic-angle spinning in one important respect. Spinning sidebands are centered about the isotropic frequency of each resonance whereas the echo spikes are centered about 0 frequency in the spectrum.

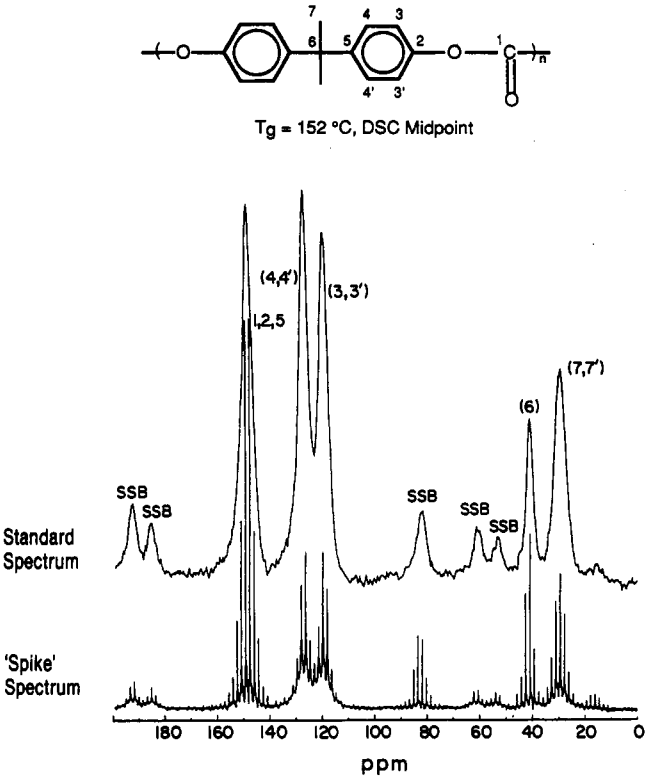

Figure 2. Spectra of Lexan 145 taken at room temperature. The top spectrum was derived in the standard fashion from a signal generated with cross polarization. The bottom spectrum was generated from a spin-echo train. Because relatively slow spinning was used for both spectra, there are prominent spinning sidebands.

The difference between the echo spectrum and a standard spectrum can be appreciated if attention is focused on the spectrum from a single type of carbon nucleus. The envelope of spikes in the echo spectrum traces out the resonance of this carbon in the standard spectrum. The width of the envelope is determined by the rate at which the corresponding signal in a single echo decays, which is the same as the rate at which the standard free-induction-decay signal decays. However, the width of the spikes themselves is determined by the rate at which the entire echo train decays. Because the spikes for carbons in different chemical environments vary in width, the relative intensities of the envelopes for chemically different nuclei may differ from the relative intensities of the corresponding resonances in the standard spectrum.

Before Fourier transformation the train of echoes was multiplied by a comb of exponential functions, having the effect of broadening the width of the envelope (usually by 15 Hz). The echo train was then multiplied by a single exponential function, having the effect of broadening the width of the spikes (usually by 1 Hz).

Results

The appearance of the spike spectrum of BPAPC depends strongly on the temperature at which the spectrum was measured (Figure 3). At temperatures slightly below room temperature the spikes of the protonated 3, 3', 4, and 4' aromatic carbons are broader than they are at 305 K. At still lower temperatures they are again sharp. The spikes of the methyl carbon are broader at low temperatures than they are at room temperature. Unlike the spikes from the aromatic carbons, the spikes from the methyl carbon are still broad at the lowest temperatures of measurement. The spikes of the quaternary 6 carbon

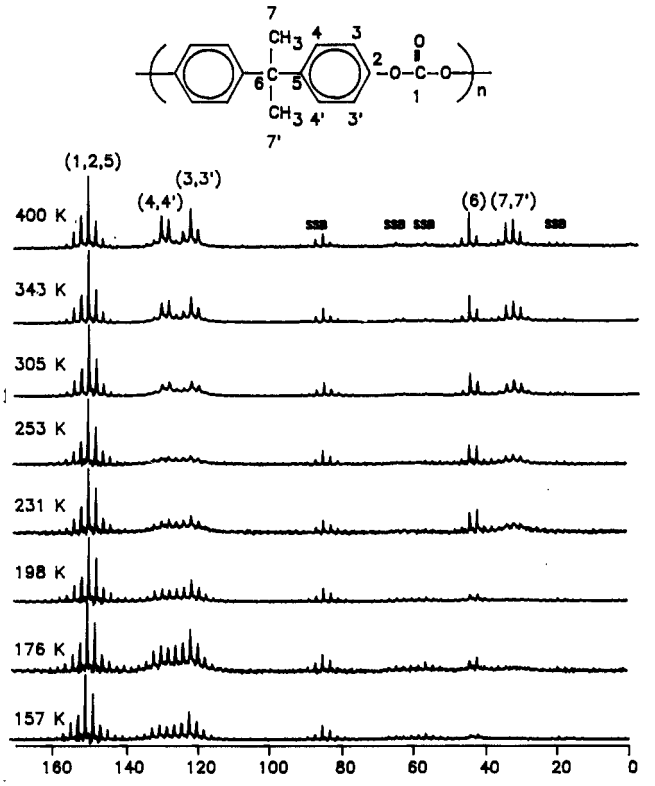

Figure 3. Temperature dependence of the ^{13}C NMR spike spectra of BPAPC. Spinning sidebands are labeled "ssb".

are slightly broader at low temperatures than at 305 K, but the spikes of the nonprotonated 2 and 5 aromatic carbons and the carbonyl carbon are just as sharp at low temperatures as they are at room temperature.

Precise measurement of the widths of the spectral spikes proved difficult, in part because the individual spikes have a non-Lorentzian shape, as would be expected for motion that is characterized by a distribution of relaxation times.[18,19] A convenient ad hoc parameter that reflects the spike width independently of the exact shape of the signals is the ratio of the height of the tallest spike in a given group to the height of the valley separating that spike and the adjacent spike. Plots of this ratio vs inverse temperature for the protonated aromatic 3 and 3′ carbons, the protonated aromatic 4 and 4′ carbons, and the methyl carbons are shown in Figures 4–6.

Initially it appeared that the temperature plots for the various samples of polycarbonate differed. Careful examination of spectra for different materials taken on the same day under identical conditions showed no variation in the results for different samples. The plots in the figures are composites for different materials.

The measured intensity ratios are subject to various experimental problems. For example, residual broadening from nonmotional sources, such as incomplete decoupling, can skew the results. The exact shape of the curves in Figures 4–6 should thus be considered qualitative. Nevertheless, the widths of the aromatic spikes clearly go through a maximum in the range of inverse temperature of (3.70–4.25) × 10^{-3} K^{-1} (235–270 K). The spikes for the methyl carbons broaden with decreasing temperature and reach an apparent plateau. The plateau is probably illusory because, once the spikes have broadened into the base line, it is no longer possible to detect changes in the spike width. The plateau simply indicates that the height of the largest spike is no greater than the noise level. For a measurement temperature of 160 K the width of the

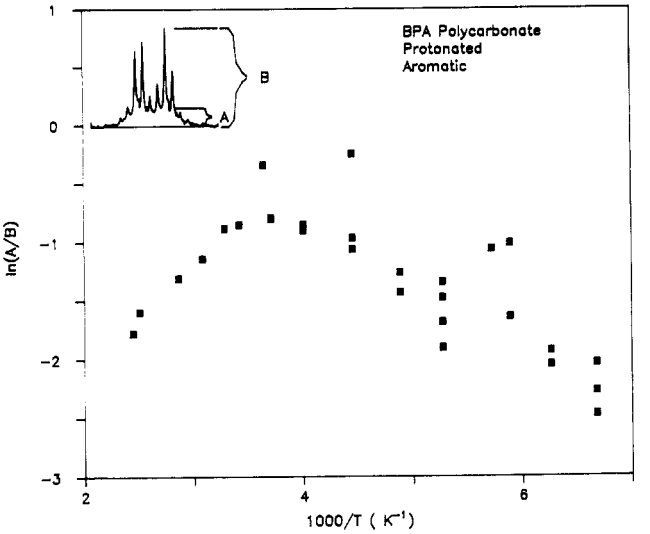

Figure 4. Temperature dependence of the peak-to-valley ratio of the spikes from the 3 and 3′ aromatic signals of BPAPC.

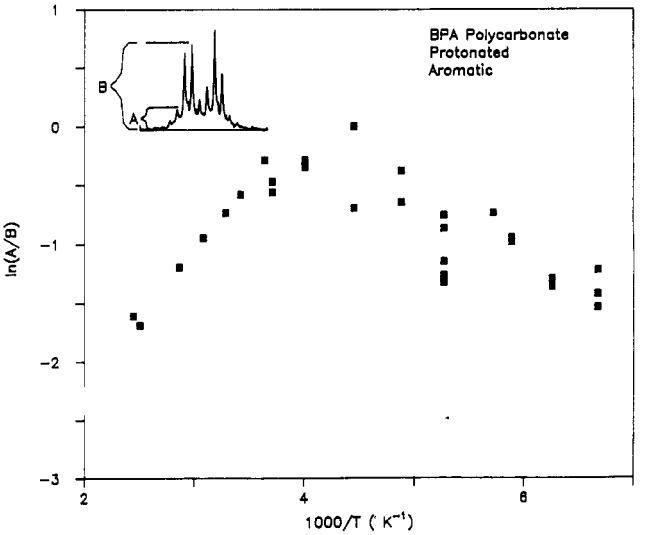

Figure 5. Temperature dependence of the peak-to-valley ratio of the spikes from the 4 and 4′ aromatic signals of BPAPC.

aromatic spikes is a modest function of the spinning rate, as is shown in Figure 7.

Discussion

Lyerla[20] reported a series of ^{13}C NMR spectra of Bisphenol A polycarbonate recorded at temperatures between 101 and 295 K. The appearance of the spectrum depends strikingly on the temperature of measurement. The methyl signal is sharp at 295 K but is very broad at 148 K. It is again sharp at 101 K. The appearance of the 3, 3′, 4, and 4′ aromatic signal also is a function of the temperature of measurement, but the changes cannot easily be characterized because of the competition between motional and nonmotional sources of line broadening.

Motional information that is obscured by nonmotional sources of line broadening in the standard spectrum clearly becomes visible in the spike spectrum. Although the spikes of the aromatic carbons are sharp at 305 K, they are broad for a measuring temperature of 253 K. For still lower temperatures the spikes are again sharp. The temperature of maximum broadening is about 250 K. The spike spectra also reflect the broadening of the methyl signals as the measuring temperature decreases.

An understanding of how best to extract the motional information in the spike spectrum requires further dis-

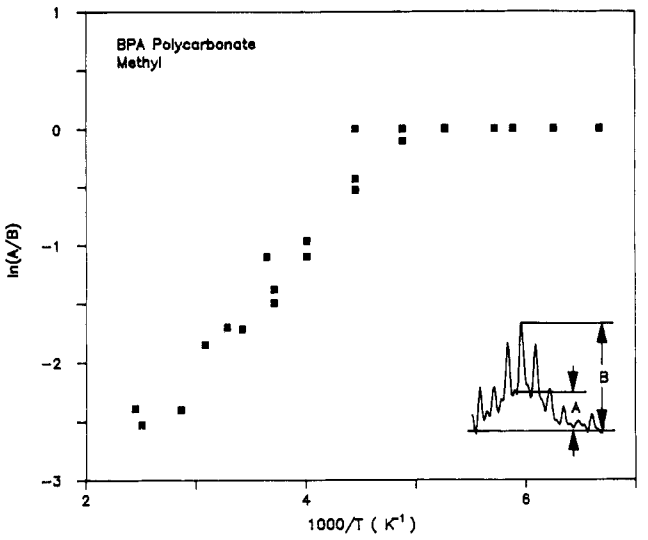

Figure 6. Temperature dependence of the peak-to-valley ratio of the spikes from the methyl signals of BPAPC.

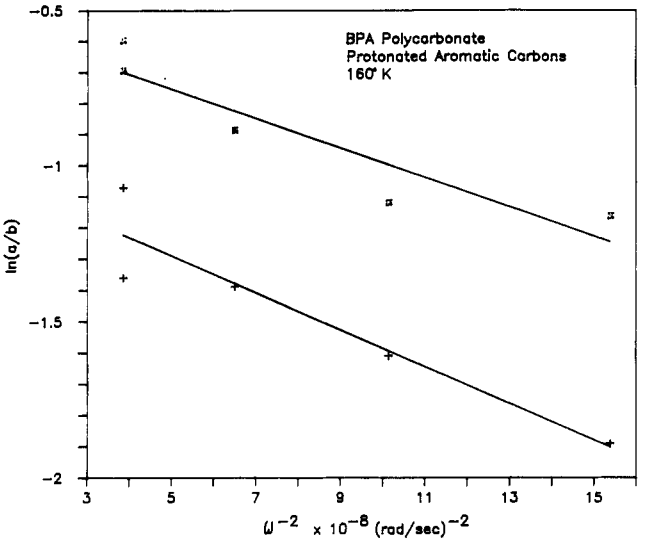

Figure 7. Spinning-rate dependence of the peak-to-valley ratio of the spikes from the protonated aromatic carbons of BPAPC.

cussion of the sources of homogeneous and inhomogeneous broadening of ^{13}C NMR signals of solids spinning at the magic angle. VanderHart and co-workers considered in detail the physical phenomena responsible for these widths.[21]

Inhomogeneous broadening in spinning samples results in part from magnetic-field inhomogeneity, missetting of the spinning angle, and bulk susceptibility effects.[21] In amorphous polymers, however, most of the inhomogeneous broadening comes from the range of absorption frequencies of the nuclei in the various individual polymer fragments situated in different local environments. Each observed NMR signal is actually a composite of the shifted signals. The inhomogeneous broadening does not usually result from molecular motion.

We will focus in the rest of the paper on the homogeneous broadening, which does derive in large part from motion. Homogeneous broadening in the ^{13}C spectra of spinning polymers generally results from processes that act on the carbon magnetizations through the carbon–proton couplings or through the chemical shift anisotropy.

Theoretical Considerations. Molecular motion creates homogeneous broadening by reducing the effectiveness of either proton decoupling or magic-angle spinning. In the absence of motion, proton irradiation reduces the effect of carbon–proton coupling by imparting a high-frequency time dependence to the interaction. The strength of the irradiation determines the period of the time dependence, and when the period is short, the interaction can effectively be ignored. But for decoupling to be effective, the carbon–proton coupling must not be changed by other processes such as molecular motion during the typical decoupling cycle. Motion that occurs on a time scale similar to the decoupling period causes transverse magnetization to decay faster than it would in the absence of motion, and this translates into broadened lines in the frequency spectrum.[22] Broadening caused by motional interference with proton decoupling is closely related to spin–lattice relaxation in the rotating frame as is explained in Appendix B.

Motional interference with magic-angle spinning occurs in much the same way as does motional interference with proton decoupling. For magic-angle spinning to remove the effect of chemical shift anisotropy on the spectrum, the individual molecular fragments must maintain a constant orientaion relative to the sample container during the average spinner revolution.[23] Equations relating carbon line widths to motion are derived in Appendix A.

Maximal interference with proton decoupling occurs when motion occurs on a time scale comparable to ω_d^{-1}, where ω_d is the angular rate at which the proton irradiation stirs the proton bath. Maximal interference with magic-angle spinning takes place when motion occurs on a time scale comparable to ω_r^{-1} where ω_r is the angular spinning rate. A typical spinning rate is $2\pi \times 5$ krad/s whereas a typical decoupling rate is $2\pi \times 50$ krad/s. A dynamic process characterized by an activation energy of 10 kcal/mol that interferes most severely with magic-angle spinning at 220 K interferes most severely with proton decoupling at 247 K. For such a small temperature difference, separate maxima in the two types of broadening probably cannot be observed. Thus broadenings from interference with magic-angle spinning and proton decoupling probably both contribute to the widths of the signals from the aromatic carbons of BPAPC at temperatures below 250 K (Figures 4 and 5).

Ring Motion in BPAPC. The aromatic rings in BPAPC undergo facile 180° flips.[19,24-29] Ring flipping is the most obvious explanation of the broadening at low temperatures of the spikes for the protonated aromatic carbons. The spikes of the nonprotonated carbons, which lie on the axis of ring rotation, will not be affected by ring flipping.

At the temperature of maximal spike broadening, 270 K, the rate of ring flipping is close to $4\pi \times 50\,000$ s^{-1}, the effective rate associated with proton decoupling affected by a two-site hopping mechanism. Activated complex theory[30] then indicates that the free energy of activation at that temperature is 8.6 kcal/mol. Deuterium[18] and carbon[19] NMR spectroscopies show that there is a distribution of rates for ring flipping. The distribution of activation energies associated with the distribution of rates is centered around 9.1 kcal/mol.[18]

The free energy of activation is not equivalent to the Arrhenius activation energy and need not agree. The difference between the two primarily lies in the entropy of activation, however. Presumably, the entropy of activation for ring flipping is small enough to be ignored. Thus the free energy of activation should be close to the Arrhenius activation energy. The activation energies from deuterium and carbon NMR are in reasonable agreement.

Recent work has shown that ring flipping is slow enough at temperatures below 125 K that separate signals for nonequivalent aromatic carbons separated by about 100 Hz can be resolved.[31] Resolution of signals from two exchanging sites takes place when the exchange rate is less than about $\pi\Delta\nu/\sqrt{2}$ s^{-1}, where $\Delta\nu$ is the spectral separation in the absence of exchange.[32] If the rate of ring flipping is $4\pi \times 50\,000$ s^{-1} at 270 K and the activation energy is 8.6 kcal/mol, the rate of ring flipping at 179 K is 314 s^{-1}. Ring flipping is slow enough that separation of the resolved signals should have begun at this temperature. Nevertheless, complete resolution of the aromatic signals takes place at some temperature below 179 K because of the distribution of correlation times for ring flipping.[33] If the rings in some sites have an activation energy of only 7.0 kcal/mol for ring flipping, the rate of flipping at those sites does not reach 314 s^{-1} until a temperature of 147 K. Full resolution of the spectrum occurs at still lower temperatures as the signals actually become sharp.

The behavior of the spin-echo spikes in the temperature region of maximum broadening can be used to limit the size of the distribution of correlation times. Calculations of the type outlined in Appendices A and B indicate that the maximum broadening caused by interference of ring flipping with proton decoupling is about 1 kHz. Ring flipping that occurs at a rate 1 order of magnitude either slower or faster than the optimum value causes broadening of 0.2 that at the maximum. We consider that the spikes are broadened into the base line when their width is comparable to the spacing between the spikes, which is 52 Hz. Thus complete disappearance of the ^{13}C signal is consistent with a distribution of correlation times for ring flipping of no more than about 2 orders of magnitude.

Although most of the results are consistent with a primary activation energy of 8.6 kcal/mol, such a high value should lead to slopes of the curves in Figures 4 and 5 that are much greater than is actually observed. The apparent activation energies are only 2–3 kcal/mol. Several explanations are possible. The presence of broadening from interference with magic-angle spinning and proton decoupling acting together reduces the temperature dependence that would be observed for either process alone. A distribution of activation energies or entropies also reduces the temperature dependence of the observed line width and can lead to an apparent activation energy that is much too low. We know that a distribution of activation energies exists,[33] and computer simulations of the line shapes shows that the slope is lowered the required amount without other unaccountable consequences for the observable data. Finally, there are significant nonmotional contributions to the spectral line widths. Measurements on rigid model compounds comparable to BPAPC show that the nonmotional contribution to the spike width of the protonated aromatic carbons is about 5 Hz. At some temperatures this is a comparable contribution to that from motion. As the spikes sharpen with increasing temperature, the nonmotional component becomes increasingly important, and the apparent temperature dependence of the spike width is reduced. Thus it appears that reliable estimates of activation energies for polymer chain motion from the spike spectra may be difficult.

Methyl Motion in BPAPC. Deuterated methyl groups in BPAPC undergo facile 3-fold rotation.[33] The activation energy is about 4.3 kcal/mol. The activation parameters from deuterium NMR spectroscopy suggest that at 160 K methyl rotation should interfere maximally with proton decoupling. In fact, Lyerla and co-workers observed the broadest methyl signals at about 160 K.[20]

The methods of Appendices A and B indicate that the maximum broadening of the carbon in a rotating methyl group is about 1500 Hz at a decoupling power of 50 kHz. If the activation energy for methyl rotation is 4.3 kcal/mol, line broadening at 230 K from methyl rotation should be about 3% of that at the maximum, or 25 Hz. This is approximately the amount to which the signals in the spike spectrum are broadened. Thus the carbon results are consistent with the deuterium results in showing that 3-fold methyl rotation is sufficient to account for most of the observed line broadening.

Nevertheless, the results of dipolar rotational spin-echo carbon NMR spectroscopy at room temperature could be matched only with the inclusion of approximately 15° isotropic motion of the methyl groups in addition to 3-fold rotation.[34] How can this be reconciled with the spin-echo results at lower temperature, which are fully explained by methyl rotation alone? Any motion of the methyl groups other than 3-fold rotation should have a temperature-dependent amplitude, either because it involves librational motion in a potential well or because it involves hopping between sites of unequal population. If the amplitude of this motion is only 15° at room temperature, it probably is too small to have a significant effect on either the deuterium or the carbon spectrum at low temperature. Indeed, 15° of motion would be difficult to detect in the deuterium spectrum in any case.

The barrier to methyl rotation in BPAPC of between 4 and 5 kcal/mol[33] is unusually high. Likewise there is a distribution of correlation times for methyl rotation spanning about 2 orders of magnitude. Methyl rotation, acting alone, should disturb the surrounding matrix very little, and chain packing should be unimportant in determining the rate of methyl rotation at a particular site. There should be a narrow distribution of rotation rates. The high barrier and distribution of rates suggest that 3-fold rotation of the methyl is coupled to motion of the aromatic rings. A requirement that methyl rotation be coupled with ring motion would raise the effective barrier for methyl rotation. The effect of chain packing on the rate of ring motion accounts for the distribution of rates for methyl rotation.

Conclusion

The spike spectra provide a very convenient means to bring out motional effects in the ^{13}C spectra of BPAPC. The temperature dependence of the line widths of BPAPC is consistent with a free energy of activation of 8–9 kcal/mol and a distribution of rates for ring flipping spanning about 2 orders of magnitude.

Acknowledgment. We are very grateful to Dr. James R. Lyerla of the IBM Research Laboratory for supplying us with a copy of his variable-temperature spectra of BPAPC.

Appendix A. Theoretical Relation between the Rate of Molecular Reorientation and NMR Spectral Line Widths in Solids

Fast Magic-Angle Spinning. The discussion below specifically treats the case of motional interference with magic-angle spinning. The equations for motional interference with proton decoupling are similar.

Reorientation is most easily described in reference to a "motional frame", chosen to take maximum advantage of the symmetry of the motion. For 180° flips of an

aromatic ring, for example, the motional frame is conveniently picked so that one axis lies along the flipping axis and the ring lies within the plane defined by that axis and one of the other axes.

Initial analysis of the effect of motion is made with respect to a motional frame having an arbitrary orientation with respect to the magnetic field. An ensemble average is then performed over all possible orientations of the molecule with respect to this frame. Ultimately the results for a multitude of orientations of the motional frame with respect to the laboratory frame are integrated.

The equation describing the time dependence of the ensemble-averaged density matrix, $\bar{\rho}(t)$, in a particular motional frame is

$$d\bar{\rho}/dt = -i\overline{[\mathcal{H}_1(t),\rho(0)]} - \int_0^t \overline{[\mathcal{H}_1(t),[\mathcal{H}_1(t-\tau),\rho(t-\tau)]]}\, d\tau \quad (1)$$

where $\mathcal{H}_1(t)$ is the Hamiltonian in the interaction representation[35] and the bar represents the ensemble average over all molecular orientations within the motional frame. The time dependence of $\bar{\rho}(t)$ and $H_1(t)$ includes high-frequency oscillation at multiples of the Larmor frequency in the interaction representation,[36] oscillation at multiples of the spinning frequency, and stochastic reorientation of the molecular fragments. Equation 1 differs from eq 32 on p 276 of the book by Abragam[36] in that the explicit time dependence of the density matrix is retained within the integral; *it is an exact expression.*

In terms of spherical tensor operators,[35] the Hamiltonian for a particular molecular orientation can be written[37]

$$\mathcal{H}_1(t) = \sum_m A_m(t)\, T_{2m} \quad (2)$$

where the time-dependence of the Hamiltonian induced by magic-angle spinning and the reorientation process is completely absorbed into the coefficients $A_m(t)$. In the interaction representation[35] oscillations at m times the Larmor frequency also contribute to the time dependence of the $A_m(t)$.[36] The coefficients contain a secular part only if the various sources of time dependence counterbalance each other. We are interested in relatively slow motions that have essentially no spectral density at the Larmor frequency. Thus our attention can be limited to the term for which $m = 0$. Without explicit designation, $\mathcal{H}_1(t)$ will refer in the rest of the paper to this truncated Hamiltonian.

Let us now expand the coefficients of this term and the density matrix in Fourier series in the spinning frequency ω_r.

$$\mathcal{H}_1(t) = \sum_{k\neq 0} a_{k0}(t)\, T_{20} \exp(-ik\omega_r t) \quad (3)$$

$$\rho(t) = \sum_j r_j(t) \exp(-ij\omega_r t) \quad (4)$$

Note that we eliminate the term for which $k = 0$ from the expansion for the Hamiltonian because we are working in an interaction representation[35] that rotates at the isotropic frequency (the rotating frame).

Substitution of eqs 3 and 4 into eq 1 leads to

$$d\bar{\rho}/dt = -i\overline{[\mathcal{H}_1(t),\rho(0)]} - \int_0^t \sum_{k,k'\neq 0}\sum_j \overline{a_{k0}(t)\, a_{k'0}(t-\tau)\, [T_{20},[T_{20},r_j(t-\tau)]]} \times \exp[-i(k+k'+j)\omega_r t] \exp[i(k'+j)\omega_r \tau]\, d\tau \quad (5)$$

In the case of interest, $\omega_r^{-1} \gg |\mathcal{H}_1|$. We will assume that $r_0(t)$ is the most significant coefficient in the series expansion of the density matrix because, with fast spinning, sidebands in the spectrum are small. Likewise, we consider only that portion of the Hamiltonian in the first term on the right-hand side of eq 5 for which $k = 0$. The other parts of the Hamiltonian are the source of the oscillation in the density matrix that we are ignoring. In the time average the stationary part of the Hamiltonian vanishes in the ensemble average so that the entire term can be ignored.

Setting $j = 0$ in eq 5 and eliminating the first term gives

$$d\bar{r}_0(t)/dt = -\sum_{k,k'\neq 0} \exp(-i(k+k')\omega_r t) \times \int_0^t \overline{a_{k0}(t)\, a_{k'0}(t-\tau)\, [T_{20},[T_{20},r_0(t-\tau)]]} \exp(ik'\omega_r \tau)\, d\tau \quad (6)$$

The exponential function in front of the integral is another source of oscillatory terms in the expansion of the density matrix. Accordingly we set $k = -k'$ because, again, we are fixing our attention on the nonoscillatory part associated with the spectral center band. We are left with

$$d\bar{r}_0(t)/dt = \sum_{k\neq 0} \int_0^t \overline{a_{k0}(t)\, a_{-k0}(t-\tau)\, [T_{20},[T_{20},r_0(t-\tau)]]} \times \exp(-ik\omega_r \tau)\, d\tau \quad (7)$$

where $r_0(t)$ now evolves slowly with time compared with the $a_{k0}(t)$. As justified by the arguments in Abragam,[36] we can perform separate ensemble averages on the operators within the integrand and the functions in $a_{k0}(t)$, pull the operators outside of the integral, and extend the limit on the integral to infinity to get

$$\frac{d\bar{r}_0(t)}{dt} = -\sum_{k\neq 0} [T_{20},[T_{20},\bar{r}_0(t)]] \int_0^\infty \overline{a_{k0}(t)\, a_{-k0}(t-\tau)} \times \exp(-ik\omega_r \tau)\, d\tau \quad (8)$$

From eq 8 it is permissible to write[38]

$$\frac{d\langle \mathbf{I}_+\rangle}{dt} = -\sum_{k\neq 0} \langle [T_{20},[T_{20}\mathbf{I}_+]]\rangle \int_0^\infty \overline{a_{k0}(t)\, a_{-k0}(t-\tau)} \times \exp(-ik\omega_r \tau)\, d\tau$$

$$= -\langle \mathbf{I}_+\rangle \frac{2}{3}\left(\frac{\omega_0}{\gamma}\right)^2 \sum_{k\neq 0} \int_0^\infty \overline{a_{k0}(t)\, a_{-k0}(t-\tau)} \times \exp(ik\omega_r \tau)\, d\tau$$

$$= -T_2^{-1}\langle \mathbf{I}_+\rangle \quad (9)$$

where ω_0 is the Larmor frequency, and $\langle \mathbf{I}\rangle$ signifies Tr $(\mathbf{I}\rho)$, where $\mathbf{I}$ is an operator. The spectral line width is $1/(\pi/T_2)$.

Details of a particular type of motion are expressed in differences in the functions $\overline{a_{k0}(t)\, a_{-k0}(t-\tau)}$, which provide a definition for correlation functions $g_{-k}(t)$. The specific

form of $g_{-k}(t)$ is [36]

$$g_{-k}(t) = \int_{\Omega_1}\int_{\Omega_2} p(\Omega_1,t-\tau)\, P(\Omega_1,t-\tau;\Omega_2,t) \times a_{k0}(\Omega_2)a_{-k0}(\Omega_1)\, d\Omega_1\, d\Omega_2 \quad (10)$$

where $p(\Omega_1,t)$ is the probability of the molecular axis system having an orientation in the motional frame specified by the set Ω_1 of Euler angles at time t and $P(\Omega_1,t-\tau;\Omega_2,t)$ is the conditional probability of the molecular axis system having orientation Ω_2 at time t if it had orientation Ω_1 at time $t-\tau$. We now treat the function $a_{k0}(\Omega_2)$ in terms of the set of Euler angles Ω_i rather than explicitly in terms of time. In stationay systems the correlation function is

$$g_{-k}(\tau) = \int_{\Omega_1}\int_{\Omega_2} p(\Omega_1,0)\, P(\Omega_1,0;\Omega_2,\tau) \times a_{k0}(\Omega_2,\tau)\, a_{-k0}(\Omega_1,0)\, d\Omega_1\, d\Omega_2 \quad (11)$$

In the case of molecular jumps among a set of discrete orientations, the integrals in eq 11 must be replaced by summations. The set of conditional probability functions in eq 11 can be arranged into a matrix $\mathbf{P}(t)$. We assume that the time dependence of $\mathbf{P}(t)$ is determined by[39]

$$d\mathbf{P}(t)/dt = \Gamma\cdot\mathbf{P}(t) \quad (12)$$

where Γ is a stochastic exchange matrix. The solution of eq 12 is[39]

$$\mathbf{P}(t) = \mathbf{P}(0)\exp(\Gamma t) \quad (13)$$

The case of interchange between two orientations (not necessarily present in equal amounts) is illustrative

$$\Gamma = \begin{pmatrix} -k_1 & k_2 \\ k_1 & -k_2 \end{pmatrix} \quad (14)$$

where k_i is the rate constant of a jump from orientation i.[39]

For each value of k_1 and k_2 we arrange the values of $a_{-k0}(\Omega_2,\tau)$ and $a_{k0}(\Omega_1,0)$ corresponding to the two orientations that are exchanged into row and column vectors $\mathbf{A}_{-k0}$ and $\mathbf{A}_{k0}$. Then

$$g_{-k}(\tau) = \mathbf{A}_{k0}\exp(\Gamma t)\mathbf{P}(0)\,\mathbf{A}_{-k0} \quad (15)$$

Diagonalization of the exchange matrix and replacement of the matrices in eq 15 with summations gives (after some algebra)

$$g_{-k}(t) = [p(\Omega_1,0)\, a_{k0}(\Omega_1) + p(\Omega_2,0)\, a_{k0}(\Omega_2)] \times [p(\Omega_1,0)\, a_{k0}(\Omega_1) + p(\Omega_2,0)\, a_{-k0}(\Omega_2)] + p(\Omega_1,0)\, p(\Omega_2,0)[a_{k0}(\Omega_2) - a_{k0}(\Omega_1)][a_{-k0}(\Omega_2) - a_{-k0}(\Omega_1)] \times \exp[-(k_1+k_2)t] \quad (16)$$

If the interaction representation[35] has been properly chosen (that is, if the rotating frame turns at the average frequency), the first term is 0. Furthermore, $a_{k0}(t) = a_{-k0}{}^*(t)$. Thus

$$g_{-k}(t) = p(\Omega_1,0)\, p(\Omega_2,0)\, |a_{k0}(\Omega_2) - a_{k0}(\Omega_1)|^2 \times \exp[-(k_1+k_2)t] = \Delta_{k0}\exp[-(k_1+k_2)t] \quad (17)$$

Motions involving more than two sites are treated by Torchia and Szabo.[37]

Slow Magic-Angle Spinning. For slow spinning the oscillatory part of the density matrix and Hamiltonian cannot be ignored. The problem is better handled with Floquet theory than with BPP.[36] Because our concern is primarily with the case in which spinning is fast, we will not develop the full analysis here for slow spinning.

Interference of Motion with Proton Decoupling. For heteronuclear dipolar coupling, only the term for $m = 0$ need be considered in eq 2. In the appropriate interaction frame in which the proton z axis is aligned along the irradiation magnetic field the Hamiltonian has the form

$$\mathcal{H}_1(t) = (2/3)^{1/2}A_0(t)\,\mathbf{I}_0[\mathbf{S}_+\exp(i\omega_1 t) + \mathbf{S}_-\exp(-i\omega_1 t)] \quad (18)$$

where $A_0(t) = C^D\rho_0 D_{00}^{(2)}[\theta(t)]$, $D_{00}^{(2)}[\theta(t)] = [3\cos^2\theta(t) - 1]/2$, $C^D = -2\hbar\gamma_I\gamma_S$, $\rho_0 = (3/2)^{1/2}r^{-3}$, and $\omega_1 = \gamma_S B_1$ where B_1 is the irradiation strength of the proton decoupling in frequency units. Then the master equation for relaxation becomes

$$d\bar{\rho}/dt = -\frac{2}{3}\int_0^t \overline{A_0(t)\, A_0(t-\tau)\, [\mathbf{B}(t),[\mathbf{B}(t-\tau),R_j(t-\tau)]]}\, d\tau \quad (19)$$

where $\mathbf{B}(t) = (\mathbf{I}_0\mathbf{S}_+\exp(i\omega_1 t) + \mathbf{I}_0\mathbf{S}_-\exp(-i\omega_1 t)$ and the first term on the right is dropped. In expanding eq 19 we drop the oscillating terms containing t to get

$$d\bar{\rho}/dt = -\frac{2}{3}\int_3^t \overline{A_0(t)\, A_0(t-\tau)}\, \{[\mathbf{I}_0\mathbf{S}_-,[\mathbf{I}_0\mathbf{S}_+,\rho(t-\tau)]] \times \exp(i\omega_1\tau) + [\mathbf{I}_0\mathbf{S}_+,[\mathbf{I}_0\mathbf{S}_-,\rho(t-\tau)]]\exp(+i\omega_1\tau)\}\, d\tau \quad (20)$$

Extending the integral gives

$$d\bar{\rho}/dt = -\frac{2}{3}\{[\mathbf{I}_0\mathbf{S}_-,[\mathbf{I}_0\mathbf{S}_+,\rho(t)]] + [\mathbf{I}_0\mathbf{S}_+,[\mathbf{I}_0\mathbf{S}_-,\rho(t)]]\} \times [2\int_0^\infty \overline{A_0(t)\, A_0(t-\tau)}\cos(\omega_1\tau)\, d\tau] \quad (21)$$

which leads to

$$d\langle\mathbf{I}_+\rangle/dt = -\langle\mathbf{I}_+\rangle(\hbar\gamma_I\gamma_S r^{-3})^2[2\int_0^\infty \overline{D_{00}^{(2)}[\theta(t)]\, D_{00}^{(2)}[\theta(t-\tau)]} \times \cos(\omega_1\tau)\, d\tau \quad (22)$$

or

$$d\langle\mathbf{I}_+\rangle/dt = -\langle\mathbf{I}_+\rangle T_2^{-1} \quad (23)$$

Thus the line width is related to a cosine transform of a correlation function describing the nature of the motion. The methods of Torchia and Szabo[37] can be used in evaluation of the correlation function.

In samples spinning at the magic angle there generally will be a distribution of line widths associated with the differing orientations of the molecules with respect to a frame fixed on the spinner. Spinning will partially average these line widths. An approximation of the width of the overall, non-Lorentzian signal can be obtained with a simple average of the remaining line widths. The approximate nature of this number should, nevertheless, be kept in mind during an analysis based on it.

Effect of the Spin-Echo Train. In principle, molecular reorientation taking place on a time scale comparable to the echo spacing could contribute directly to echo decay. Many rotations of the sample container occur between each pair of pulses, however. Likewise the proton irradiation churns the spin system many times during one turn of the container. The chemical shift anisotropy and carbon–proton decoupling will both be reduced to zero before random reorientation can interfere if the stochastic process occurs at a rate comparable to the rate of radio-frequency pulsing. Thus direct interference of motion on the formation of the spin echoes is not important. Rather the spin-echo experiment serves as a convenient means by which the direct interference of reorientation on the spinning and decoupling processes may be observed through the indirect effect on the spin echoes.

Appendix B. Relation between ^{13}C NMR Spectral Line Widths and Spin–Lattice Relaxation in the Rotating Frame

The rate at which carbon transverse magnetization decays in the presence of proton irradiation (decoupling) is closely related to the rate at which spin-locked carbon magnetization decays in a $T_{1\rho}$ measurement. In the former case time dependence is imparted to the carbon–proton interaction by irradiation of the protons; in the latter it is created by irradiation of the carbons. The frequency at which the coupling is modulated is equal in both cases if the power levels of the two channels have been set for a cross-polarization experiment. If there are no nonmotional contributions to $T_{1\rho}$ relaxation

$$2T_{1\rho}^{-1} = \Delta\omega_d \tag{24}$$

where $\Delta\omega_d$ is the carbon line width attributable to motional interference with decoupling.[21]

An important nonmotional contribution to $T_{1\rho}$ results from modulation of the carbon–proton coupling interaction by spin flips caused by strong coupling of the various protons in the polymer to each other.[34,40] In many polymers, however, especially those in which there is a low proton density, $T_{1\rho}$ relaxation is dominated by motional effects.[34,41] Procedures are available for estimation of the importance of proton–proton interactions in doubtful cases.[42] Interestingly, the interproton interactions are scaled down when the proton system is irradiated but not when the carbons are irradiated. Thus carbon line widths measured in the presence of proton decoupling are more likely to be motionally determined than are $T_{1\rho}$ relaxation times measured with carbon relaxation.

Appendix C. Relation between a Distribution of Correlation Times and Distributions of Activation Parameters

It is well-known that kinetic processes in amorphous polymers must be described in terms of a distribution of correlation times. For processes that involve interchange among discrete states, the correlations times are inversely related to the rate constants for interchange between states, and a distribution of correlation times translates into a distribution of rate constants k (or more conveniently, into a distribution of ln k).

Each rate constant in the distribution is related to an activation energy by the Arrhenius relation.

$$k = k_0 \exp(-E_a/RT) \tag{25}$$

It is tempting to interpret the distribution of rate constants in terms of a distribution of activation energies, E_a. Equally plausible, however, is a distribution of prefactors, k_0.

Activated complex theory shows that a distribution in activation energies is equivalent to a distribution in activation enthalpies. A distribution in prefactors is equivalent to a distribution of activation entropies.

If there is a distribution of activation energies, the width in the distribution of ln k scales inversely with temperature. If there is a distribution of prefactors, the width of the distribution of ln k is temperature independent. Thus, in principle, it is possible to differentiate between the two possibilities. In real circumstances, of course, there is probably a combination of a distribution in prefactors and activation energies.

References and Notes

(1) Schaefer, J.; Stejskal, E. O.; Steger, T. R.; Sefcik, M. D.; McKay, R. A. *Macromolecules* **1980**, *13*, 1121.
(2) Sacher, E. *J. Macromol. Sci., Phys.* **1975**, *B11* (3), 403.
(3) Sacher, E. *J. Macromol. Sci., Phys.* **1874**, *B10* (2), 319.
(4) Heijboer, J. *J. Polym. Sci., Part C* **1968**, *16*, 3755.
(5) Boyer, R. F. *Polym. Eng. Sci.* **1968**, *8*, 161.
(6) Freeman, R.; Hill, H. D. W. In *Dynamic Nuclear Magnetic Resonance Spectroscopy*; Jackman, L. M., Cotton, F. A., Eds.; Academic: New York, 1975.
(7) Frye, J. S.; Maciel, G. E. *J. Magn. Reson.* **1982**, *48*, 125.
(8) Olejniczak, E. T.; Vega, S.; Griffin, R. G. *J. Chem. Phys.* **1984**, *81*, 4804.
(9) Raleigh, D. P.; Olejniczak, E. T.; Vega, S.; Griffin, R. G. *J. Magn. Reson.* **1987**, *72*, 238.
(10) Hemminga, M. A.; de Jaeger, P. A. *J. Magn. Reson.* **1983**, *51*, 339.
(11) Dixon, W. T. *J. Chem. Phys.* **1982**, *77*, 1800.
(12) VanderHart, D. L.; Garroway, A. N. *J. Chem. Phys.* **1979**, *71*, 2773.
(13) Garroway, A. N. *J. Magn. Reson.* **1977**, *28*, 365.
(14) Zilm, K. Presented at the 27th Experimental NMR Conference, Baltimore, MD, April 1986.
(15) Swanson, S.; Ganapathy, S.; Henrichs, P. M.; Bryant, R. G. *J. Magn. Reson.* **1986**, *69*, 531.
(16) Maricq, M.; Waugh, J. S. *Chem. Phys. Lett.* **1977**, *47*, 327.
(17) Maricq, M. M.; Waugh, J. S. *J. Chem. Phys.* **1979**, *70*, 3300.
(18) Wehrle, M.; Hellmann, G. P.; Spiess, H. W. *Colloid Polym. Sci.* **1987**, *265*, 815.
(19) Schaefer, J.; Stejskal, E. O.; McKay, R. A.; Dixon, W. T. *Macromolecules* **1984**, *17*, 1479.
(20) Lyerla, J. R. In *High Resolution NMR Spectroscopy of Synthetic Polymers in Bulk*; Komoroski, R. A., Ed.; VCH: Deerfield Beach, FL, 1986; p 96.
(21) VanderHart, D. L.; Earl, W. L.; Garroway, A. N. *J. Magn. Reson.* **1981**, *44*, 361.
(22) Rothwell, W. P.; Waugh, J. S. *J. Chem. Phys.* **1981**, *74*, 2721.
(23) Suwelack, D.; Rothwell, W. P.; Waugh, J. S. *J. Chem. Phys.* **1980**, *73*, 2559.
(24) Spiess, H. W. *J. Mol. Struct.* **1983**, *111*, 119.
(25) Spiess, H. W. *Colloid Polym. Sci.* **1983**, *261*, 193.
(26) Roy, A. K.; Jones, A. A.; Inglefield, P. T. *J. Magn. Reson.* **1985**, *64*, 441.
(27) Inglefield, P. T.; Amici, R. M.; O'Gara, J. F.; Hung, C. C.; Jones, A. F. *Macromolecules* **1983**, *16*, 1552.
(28) O'Gara, J. F.; Jones, A. A.; Hung, C. C.; Inglefield, P. T. *Macromolecules* **1985**, *18*, 1117.
(29) Roy, A. K.; Jones, A. A.; Inglefield, P. T. *Macromolecules* **1986**, *19*, 1356.
(30) Moore, W. J. *Physical Chemistry*; 3rd ed.; Prentice-Hall: Englewood Cliffs, NJ, 1963; p 297.
(31) Henrichs, P. M.; Nicely, V. *Macromolecules* **1990**, *23*, 3193.
(32) Carrington, A.; McLachlin, A. D. *Introduction to Magnetic Resonance*; Harper and Row: New York, 1967; p 207.
(33) Schmidt, C.; Kuhn, K. J.; Spiess, H. W. *Prog. Colloid Polym. Sci.* **1985**, *71*, 71.
(34) Schaefer, J.; Sefcik, M. D.; Stejskal, E. O.; McKay, R. A.; Dixon, W. T.; Cais, R. E. *Macromolecules* **1984**, *17*, 1107.
(35) Haeberlen, U. H. *High Resolution NMR in Solids*; Academic: New York, 1976.
(36) Abragam, A. *The Principles of Nuclear Magnetism*; Oxford: New York, 1961.
(37) Torchia, D. A.; Szabo, A. *J. Magn. Reson.* **1982**, *49*, 107.
(38) Schlichter, C. P. *Principles of Magnetic Resonance*; Springer: New York, 1978.
(39) Bharucha-Reid, A. T. *Elements of the Theory of Markov Processes and Their Application*; McGraw Hill: New York, 1960.
(40) Laupetre, F.; Monnerie, L.; Virlet, J. *Macromolecules* **1984**, *17*, 1397.
(41) Schaefer, J.; Sefcik, M. D.; Stejskal, E. O.; McKay, R. A. *Macromolecules* **1984**, *17*, 1118.
(42) Schaefer, J.; Sefcik, M. D.; Stejskal, E. O.; McKay, R. A. *Macromolecules* **1981**, *14*, 280.

Registry No. BPAPC (copolymer), 25037-45-0; BPAPC (SRU), 24936-68-3.